Physical basis of spindle self-organization

Jan Brugués[a,b,c,1] and Daniel Needleman[a]

[a]School of Engineering and Applied Sciences, Department of Molecular and Cellular Biology, and FAS Center for Systems Biology, Harvard University, Cambridge, MA 021382; [b]Max Planck Institute of Molecular Cell Biology and Genetics, 01307 Dresden, Germany; and [c]Max Planck Institute for the Physics of Complex Systems, 01187 Dresden, Germany

Edited by Boris I. Shraiman, University of California, Santa Barbara, CA, and approved November 7, 2014 (received for review May 29, 2014)

The cytoskeleton forms a variety of steady-state, subcellular structures that are maintained by continuous fluxes of molecules and energy. Understanding such self-organizing structures is not only crucial for cell biology but also poses a fundamental challenge for physics, since these systems are active materials that behave drastically differently from matter at or near equilibrium. Active liquid crystal theories have been developed to study the self-organization of cytoskeletal filaments in in vitro systems of purified components. However, it has been unclear how relevant these simplified approaches are for understanding biological structures, which can be composed of hundreds of distinct proteins. Here we show that a suitably constructed active liquid crystal theory produces remarkably accurate predictions of the behaviors of metaphase spindles—the cytoskeletal structure, composed largely of microtubules and associated proteins, that segregates chromosomes during cell division.

active matter | spindle assembly | microtubules and motors

Continuum theories form the basis of our understanding of much of the material world, but it has been unclear if such theories can be used to study self-organizing biological structures, due to the complexity and fundamentally nonequilibrium nature of these systems. One example of these structures that has been extensively studied for over a century is the metaphase spindle, an ensemble of microtubules, molecular motors, and other associated proteins that segregates chromosomes during cell division. Hundreds of proteins have been found to contribute to spindle assembly (1), but while various principles have been proposed to explain how these constituents self-organize to form the spindle—including gradients of signaling molecules (2), a mechanical matrix (3), and the regulated "feeding" of microtubule depolymerizers by microtubule sliding (4)—the physical basis of spindle assembly is currently unknown (5). Complementary to this in vivo work, in vitro experiments have shown that mixtures consisting solely of purified cytoskeletal filaments and motors can spontaneously self-organize into structures (6, 7) and display complex dynamics (8–10). Sophisticated theories of these simplified systems have been developed to explain how the collective effects of the local interactions of microtubules, mediated by motors, give rise to these large-scale behaviors (11, 12). It is unclear if the principles learned from these reconstituted systems apply to the self-organization of the spindle and other cytoskeletal structures in vivo.

Here we apply a holistic approach to study the physical principles that give rise to spindle self-organization by quantitatively studying the collective behaviors of microtubules in spindles. Our approach uses the intimate connection between spatiotemporal correlation functions of the spontaneous fluctuations of microtubule density, orientation and stress, and the underlying physical processes that drive them. Comparing measurements of the correlation function with predictions from theory provides both a rigorous test of the validity of that theory and a sensitive means of determining its parameters. Similar approaches are commonly used in condensed matter physics to quantitatively test explanations of phenomena (13) and provide the basis of several widely used experimental techniques, such as Fluorescence Correlation Spectroscopy and Dynamic Light Scattering. We therefore sought to experimentally measure correlation functions associated with density, orientation, and stress in metaphase arrested spindles assembled in *Xenopus laevis* egg extracts. All of our measurements on correlation functions and spindle morphology can be quantitatively accounted for using an active liquid crystal theory that we construct. Our combined theoretical and experimental approach provides a general framework for understanding the structure and dynamics of the spindle and its responses to physical and molecular perturbations.

We used an LC-Polscope (14), a form of polarized light microscopy, to quantitatively measure the retardance (the birefringence integrated over the optical volume) and the optical slow axis, also called the nematic director (a measure of microtubule orientation), at every pixel in time-lapse movies of spindles (Fig. 1*A* and Movies S1 and S2). LC-Polscope movies reveal that at steady state, microtubules are highly oriented along the spindle long axes, and display large orientational fluctuations (see Movie S1). We used these movies to compute the spatiotemporal correlations of director fluctuations (see *Methods Summary* and Fig. 1 *A* and *B*) and found that the equal time director autocorrelation function decays with wavelength as $1/q^2$ and decays with frequency as $1/\omega^2$ (for $q \to 0$). Fluctuations of this form indicate that nearby microtubules tend to orient in the same direction while microtubules that are farther apart are less well aligned, and are quantitatively consistent with microtubules being oriented by their local interactions from cross-linkers, motors, and steric effects (see *SI Text*) (12, 15). This form of the director autocorrelation function is inconsistent with microtubules being embedded in an elastic matrix (which would cause a plateau in the orientational correlation function at long wavelength due to elastic deformation of the matrix), or microtubules being aligned independently of each other by an external field or global signal (which would result in a flat equal time

Significance

The spindle segregates chromosomes during cell division and is composed of microtubules and hundreds of other proteins, but the manner in which these molecular constituents self-organize to form the spindle remains unclear. Here we use a holistic approach, based on quantitative measurements in spindles of the spatiotemporal correlation functions of microtubule density, orientation, and stresses, to identify the key processes responsible for spindle self-organization. We show that microtubule turnover and the collective effects of local microtubule interactions, mediated via motor proteins and cross-linkers, can quantitatively account for the dynamics and the structure of the spindle. We thus reveal the physical basis of spindle self-organization and provide a framework that may be useful for understanding cytoskeletal function in vivo.

Author contributions: J.B. and D.N. designed research; J.B. and D.N. performed research; J.B. contributed new reagents/analytic tools; J.B. and D.N. analyzed data; and J.B. and D.N. wrote the paper.

The authors declare no conflict of interest.

This article is a PNAS Direct Submission.

[1]To whom correspondence should be addressed. Email: brugues@mpi-cbg.de.

This article contains supporting information online at www.pnas.org/lookup/suppl/doi:10.1073/pnas.1409404111/-/DCSupplemental.

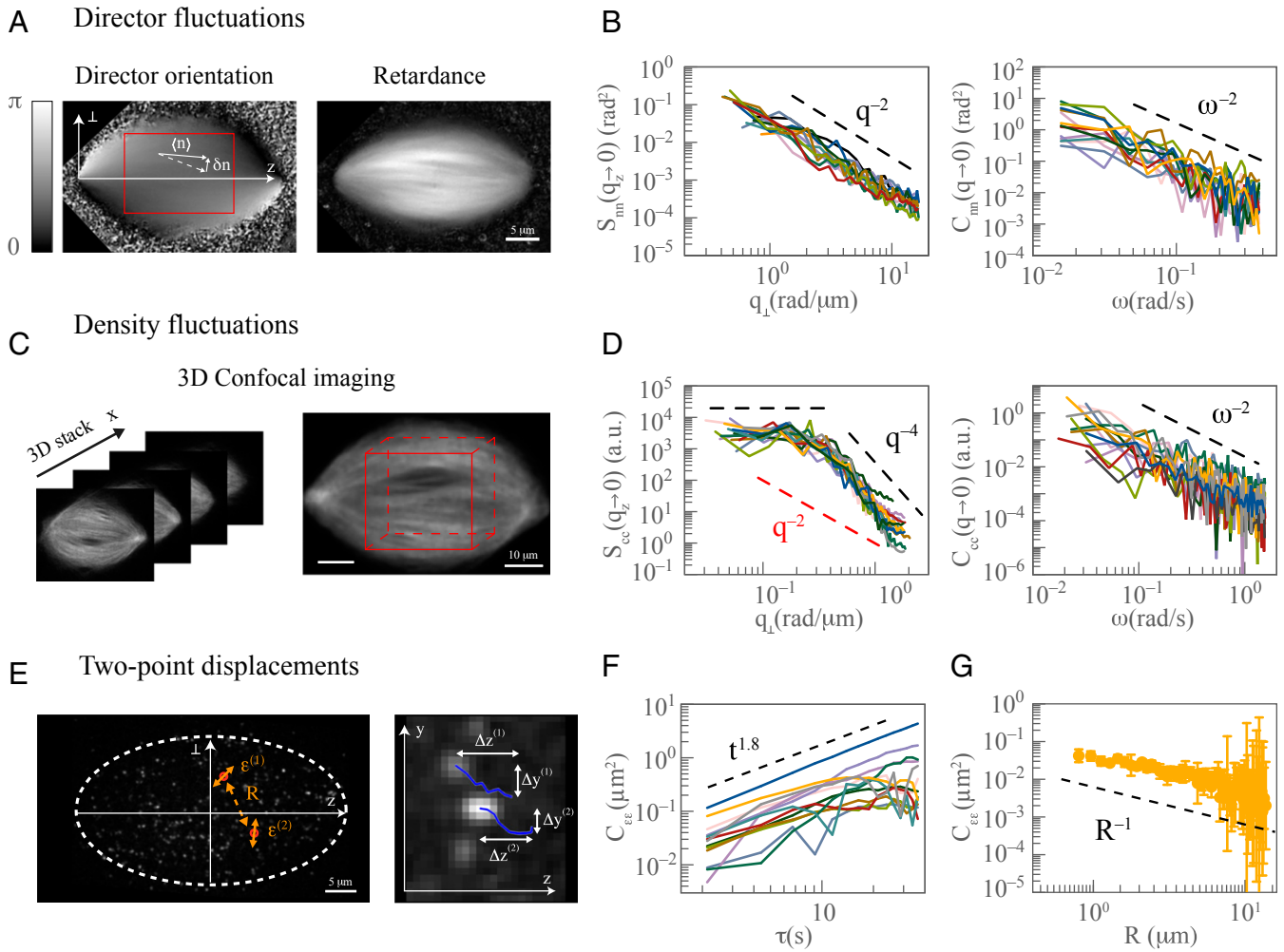

Fig. 1. Measurement of director orientation, density, and two-point correlation functions. (*A*) LC-Polscope images provide a quantitative measurement of the director orientation (*Left*) and retardance (*Right*). The red square illustrates a typical region used to calculate the spatiotemporal correlations of the orientation fluctuations (dashed white arrow) with respect to the mean orientation at that location (solid white arrow). See also Movies S1 and S2. (*B*) (*Left*) Equal time director autocorrelation functions from 14 spindles as a function of the wave number, $q_\perp$, for $q_z = 0.39$ rad/μm, the lowest wave number measured along this direction ($<< q_\perp$). Dashed line represents a $1/q_\perp^2$ decay. (*Right*) Long-wavelength limit of the spatiotemporal correlation as a function of the frequency. Dashed line represents a $1/\omega^2$ scaling. (*C*) We used 3D confocal fluorescence time-lapse movies to measure spatiotemporal correlations of the microtubule density fluctuations. The red cube illustrates a typical 3D region used to measure these correlations. See also Movie S3. (*D*) (*Left*) The amplitude of the equal time density autocorrelation function ($n = 14$ spindles) plateaus for long wavelengths and decays as$1/q_\perp^4$ for short wavelengths (dashed black lines) and in marked contrast to the $1/q_\perp^2$ scaling predicted without turnover (dashed red line). (*Right*) Long-wavelength limit of the spatiotemporal correlation. Dashed line represents a $1/\omega^2$ scaling. (*E*) (*Left*) A frame of single molecule time-lapse movie of fluorescently labeled microtubules. The dashed white contour represents the boundary of the spindle. Red circles highlight two single fluorescence molecules. Solid orange represents particle displacements ($\varepsilon^{(1)}$, $\varepsilon^{(2)}$). Orange dashed line represents distance (R) between particles. (*Right*) Detail of two speckles and their spatial displacements over time (blue line). See also Movie S4. (*F*) Cross-correlations of pairs of tracer particles ($C_{\varepsilon\varepsilon}$; see *Methods Summary*) normalized by their initial distance as a function of time lag (τ) show superdiffusive behavior. Dashed line corresponds to an exponent of 1.8; each trajectory (13 in the figure) corresponds to the average two point cross-correlations of a spindle. (*G*) Spatial dependence of the two-point cross-correlations $C_{\varepsilon\varepsilon}$ for the smallest measured time lag, $\tau = 2.1$ s, decays as $1/R$, as expected in a continuum theory.

correlation function because local fluctuations would not collectively accumulate).

We measured microtubule density in spindles by obtaining 3D time-lapse spinning disk confocal microscopy movies of spindles labeled with high concentration of fluorescent tubulin (Fig. 1*C* and Movie S3). The equal time autocorrelation function of density fluctuations along the direction perpendicular to the spindle axis (⊥) plateaus for small $q_\perp$, and decays as $1/q_\perp^4$ for large $q_\perp$ (Fig. 1*D*). The relative sliding of microtubules, by the activity of cross-linking molecular motors (16), will produce a coupling between the orientation and density of microtubules, so fluctuations in orientation will lead to fluctuations in density. If the dominant processes that controlled microtubule arrangement in the spindle were this relative sliding and the tendency of microtubules to locally orient each other, revealed from our LC-Polscope measurements, then the density fluctuations would diverge as $1/q^2$ (see *SI Text* and ref. 17), in marked contrast with their observed behavior (Fig. 1*D*). Microtubules in the spindle are also continuously being nucleated, growing, and shrinking (2). The combination of this rapid turnover with the mutual orientation and sliding of microtubules predicts density correlation functions of the form that is experimentally observed (see *SI Text*). The plateau in the density correlation function at small q arises because microtubules turn over too rapidly to be transported significant distances by sliding, so large-scale motor driven fluctuations are suppressed. The $1/q^4$ decay at short wavelengths

results from the orientation and sliding interactions cooperating with stochastic, diffusive-like motions of microtubules (an intermediate $1/q^2$ decay would be observed if either diffusion or orientation interactions dominate for intermediate wavelengths, but an appreciable regime of this nature is not seen, indicating that these two process have similar magnitudes). Thus, the scaling of the orientational and density fluctuations can be explained by the local, mutual interactions of microtubules sliding and orienting each other, while polymerizing and depolymerizing.

To study the production and propagation of forces, we measured stress fluctuations in spindles using a combination of passive two-point particle displacements and active microrheology measurements (18–20). This method relies on the generalized Stokes–Einstein equation to relate the correlated motions between pairs of particles to the mechanics of the intervening media and the stresses that drive their motion, and is valid for incompressible, viscoelastic continuous media in the presence of both active and thermal stress fluctuations (19, 20) (see *SI Text*). We obtained two-point particle displacements by tracking single molecules of fluorescently labeled tubulin incorporated into microtubules in the spindle, and computed the two-point correlation between these single molecules along the direction perpendicular to the spindle axis (see Fig. 1 *E* and *F*). The two-point displacements decay as the inverse of the particle separation, R (Fig. 1*G*), consistent with stresses being propagated by the local interactions between microtubules [and as would be expected in any media that can be approximated as a continuum (19)]. These two-point displacements exhibit super-diffusive motion with an exponent $\alpha \sim 1.8$ (Fig. 1*F*), which, when combined with the active microrheology measurements of the frequency-dependent shear modulus of the spindle by Shimamoto et al. (21), reveals that stress fluctuations in the spindle increase linearly with time lag (see below). This spectrum of stress fluctuations is expected from motors exerting forces between microtubules they cross-link, giving rise to dipolar stresses (see *SI Text* and ref. 17).

Our investigation of the scaling of spatiotemporal correlation functions of microtubule orientation, microtubule density, and stresses in the spindle reveals the role of local interactions between microtubules in orienting, sliding, and generating and propagating stresses between microtubules, as well as the importance of microtubule turnover. To more thoroughly study these phenomena, we constructed a minimal model of these processes based on the shape of the correlation functions of density, orientation, and stress that is consistent with relevant conservation laws and the known symmetries of microtubules in the spindle, and explored predictions beyond scaling (see *SI Text*). The prediction for the equal time director autocorrelation function in the perpendicular direction to the spindle is $S_\perp^2/2Kq_\perp^2$, and the frequency dependence of the director autocorrelation function (for $q \to 0$) is $S_\perp^2/\omega^2$, where $S_\perp$ is the magnitude of orientation noise (assumed Gaussian), and K is the strength of the nematic elasticity, a measure of the tendency of local interactions to orient microtubules. Thus, these two

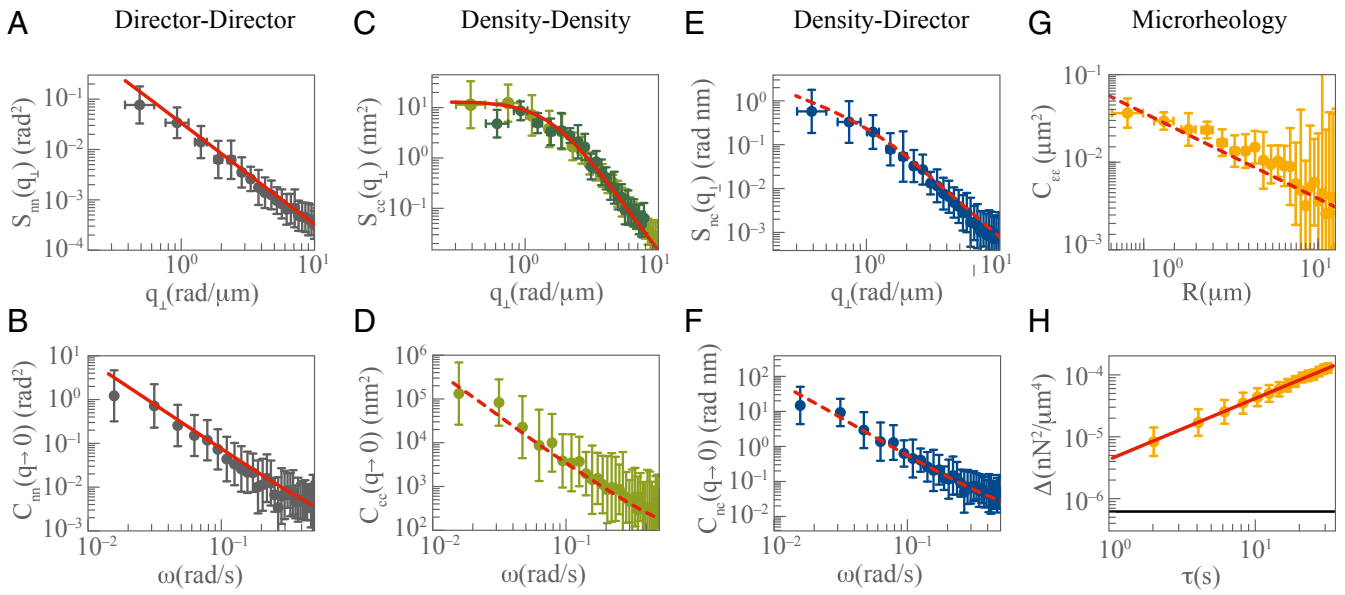

Fig. 2. Comparison between experimental data and expected periodogram of the theoretical predictions (see *Methods Summary* and *SI Text*) for density, director orientation, and stress correlation functions. Solid red lines show the fits used to determine the six parameters of the theory, and the dashed red lines are the resulting predictions. (*A*) Average equal time correlation functions for the director–director fluctuations obtained from the LC-Polscope, and corresponding fit to the theoretical prediction $S_{nn} = S_\perp^2/2Kq_\perp^2$ (solid red line). (*B*) Average frequency dependence of the spatiotemporal correlation functions for the director–director fluctuations obtained from the LC-Polscope, and corresponding fit to the theoretical prediction, $C_{nn} = S_\perp^2/(\omega^2 + K^2q_0^4)$ (solid red line), where $q_0 = 0.39$ rad/μm is the lowest wave number measured. (*C*) Average equal time correlation functions for density–density fluctuations obtained from fluorescence (Fig. 1*D*, dark green) and LC-Polscope retardance measurements (light green). The fluorescence density correlations were rescaled to the retardance correlations, which have units of square nanometers. These correlations were fit to the theoretical prediction for the equal time density correlations, $S_{cc} = \{(q_\perp^2 v_0^2 c_0^2 S_\perp^2)/[2(K^2q_\perp^4 + (\Theta + Dq_\perp^2)^2)]\}[1/Kq_\perp^2 + 1/(\Theta + Dq_\perp^2)]$ (solid red line). To convert density to number of microtubules per volume, we normalized $c_0 v_0$ by the average retardance and rescaled it to the number of microtubule per unit volume using EM images of *Xenopus* spindles (22), 7.14 microtubules/μm^3 [50 microtubules/μm^2 in a cross-section, divided by the average microtubule length in a spindle, 7 μm (23)]. (*D*) Average frequency dependence of the spatiotemporal correlation functions for density–density fluctuations obtained from the retardance measurements. These correlations agree quantitatively with the theoretical prediction for the frequency-dependent density correlations, $C_{cc} = (q_0^2 v_0^2 c_0^2 S_\perp^2)/\{(\omega^2 + K^2q_0^4)[\omega^2 + (\Theta + Dq_0^2)^2]\}$ (dashed red line). (*E* and *F*) Theoretical predictions (dashed red lines) for the equal time and frequency dependence spatiotemporal density–director cross-correlation functions, (*E*) $|S_{cn}| = (v_0 c_0 S_\perp^2)/\{2Kq_\perp[\Theta + (K + D)q_\perp^2]\}$ and (*F*) $|C_{cn}| = (v_0 c_0 q_\perp S_\perp^2)/\{(\omega^2 + K^2q_0^4)[\omega^2 + (\Theta + Dq_0^2)^2]^{1/2}\}$, respectively, and their corresponding experimental measurements. (*G*) Spatial dependence of the two-point cross-correlations for the smallest measured time lag (Fig. 1*G*) and its theoretical prediction $C_{\varepsilon\varepsilon} = A/R$, where A is a constant (see *SI Text*). (*H*) Temporal dependence of the stress fluctuations and its theoretical fit, $\Delta(\tau) = 2W^2 c_0^2 S_\perp^2 \tau$. Black line corresponds to the prediction from the fluctuation dissipation theorem. Error bars are SDs.

parameters can be determined by fitting the director correlation functions (Fig. 2 *A* and *B*) leading to $S_\perp = 0.021 \pm 0.002$ rad $s^{3/2}\cdot\mu m^{3/2}$, $K = 0.022 \pm 0.009$ $\mu m^2\cdot s^{-1}$. The measured equal time density autocorrelation function is well fit by the predicted form, $S_{cc} = \{q_\perp^2 v_0^2 c_0^2 S_\perp^2/[2(K^2 q_\perp^4 + (\Theta + D q_\perp^2)^2)]\}\cdot[1/(K q_\perp^2) + (1/\Theta + D q_\perp^2)]$ (Fig. 2*C*; see *SI Text*), which has a plateau for small q of $S_{cc} \sim v_0^2 c_0^2 S_\perp^2/2K\Theta^2$, where c_0 is the average density of microtubules, v_0 is the velocity of microtubule transport, and Θ is the turnover rate, and transitions to the $1/q_\perp^4$ regime at a wavelength determined by the square root of the ratio of K and Θ, $S_{cc} \approx [(v_0^2 c_0^2 S_\perp^2)/(2q_\perp^4)]\{(D+K)/[KD(K^2+D^2)]\}$. Thus, this fit provides a means to measure the stationary flux, $c_0 v_0 = 3.3 \pm 0.4$ microtubules $\mu m^{-2}\cdot s^{-1}$, the turnover rate, $\Theta = 0.06 \pm 0.02$ s^{-1}, and the coefficient characterizing diffusive-like motion of microtubules in the spindle, $D = 0.022 \pm 0.006$ $\mu m^2\cdot s^{-1}$ (Fig. 2*C*). This value of Θ corresponds to a microtubule turnover time of $1/\Theta \approx 17$ s, which, within error, is the same as the average lifetime of microtubules in the spindle measured from single molecule studies (24). The prediction for the spectrum of stress fluctuations, $\Delta(\omega) = 4W^2 c_0^2 S_\perp^2/\omega^2$, provides a good fit to our measurements (see Fig. 2*H* and *SI Text*), giving $Wc_0 = 69 \pm 2$ pN/μm^2, where W is the active stress per unit microtubule density. This magnitude of stress fluctuations is consistent with ~1 molecular motor per micrometer of microtubule (assuming an average force per motor of ~10 pN). The measured stress fluctuations are orders of magnitude greater, and have a different temporal dependence, than predicted from the equilibrium fluctuation dissipation relation (Fig. 2*H*, black line), based on thermal fluctuations and the measured rheology of the spindle (21). The strong violation of the equilibrium fluctuation dissipation relationship demonstrates the intrinsic out-of-equilibrium nature of the spindle. The linear temporal increase of the stress fluctuations corresponds to a $1/\omega^2$ frequency dependence, which has previously been reported for reconstituted cytoskeletal systems (25) and cells (19, 26).

As described above, if microtubule movements are driven by their mutual, local interactions, then the orientation and density of microtubules will be coupled. This coupling should be fundamental for driving the dynamics of microtubules in the spindle because large orientational fluctuations, which result from the collective accumulation between microtubules, should dominate other sources of density fluctuations. To explore the validity of these ideas and to directly probe this coupling, we sought to measure the cross-correlation between microtubule density and orientation in the spindle. To experimentally determine density–director cross-correlations, it is necessary to simultaneously measure both these fields, which is possible using the pair of images simultaneously provided by the LC-Polscope: The orientation of the optical slow axis is the orientation of the director, while the retardance is proportional to microtubule density, as expected from of the high degree of ordering of microtubules in spindles and as is directly demonstrated by the quantitative agreement between the retardance and fluorescence autocorrelation functions (Fig. 2*C*). The measured equal time and frequency-dependent (for $q \to 0$) density–director cross-correlations are in quantitative agreement with predictions using the previously measured parameters (Fig. 2 *E* and *F*), thus strongly supporting the validity of the proposed mechanisms. Alternatively, simultaneously fitting all eight correlation functions (wavelength and frequency dependence of density–density, director–director, density–director, and stress) does not significantly change the results. Explaining these eight correlation functions with a theory with only six parameters is a strong validation of the theory because even if all of the correlation functions were simple power laws (and they actually display more complex structure), it would be necessary to use 16 free parameters to empirically characterize the measured curves. In conclusion, all of our quantitative measurements of microtubule orientation, density, and the generation and propagation of stress in the spindle are consistent with spindle self-organization arising from the local interactions of microtubules, mediated by cross-linkers and motors, and microtubule polymerization dynamics.

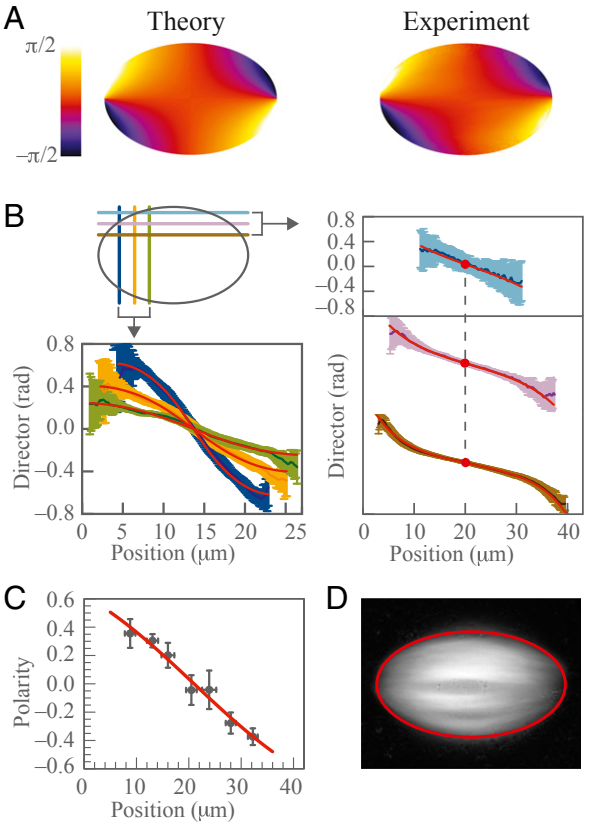

Fig. 3. Shape of the spindle: director orientation, polarity, and boundary. (*A*) Prediction of director orientation in the spindle (*Left*) and corresponding measurement (*Right*) from averaging ~5 min of an LC-Polscope movie (100 frames) of a spindle. (*B*) Spatial dependence of director orientation for several sections in the spindle. Red dot in right plot corresponds to the same orientation value in the three sections. Error bars correspond to SDs. (*C*) Polarity measurements from ref. 23 and corresponding theoretical fit. (*D*) Representative retardance image of a spindle with the best fit to an ellipse (solid red).

Having shown that the local interactions of microtubules and microtubule turnover are sufficient to account for the internal dynamics of the spindle, we next sought to investigate if these same processes could explain the morphology of the spindle. In this view, the spindle is similar to a droplet of liquid crystal, but it is composed of a nonequilibrium material with properties determined from our measurements of correlation functions. Building off of theories of the shape of liquid droplets (27, 28), appropriately modified to account for the active nature of the spindle, we approximated the spindle as an ellipse with constant density and fixed volume, and calculated the distribution of microtubule orientation and polarity inside the spindle and the aspect ratio of the spindle. The orientation of microtubules is governed by nematic elasticity—arising from the tendency of microtubules to mutually align each other—and is thus solely determined by the solution of Laplace's equation with the appropriate geometry and boundary conditions, which we take to be tangential anchoring with two half defects at the poles (see *SI Text*). The calculated orientation of microtubules throughout the spindle quantitatively agrees with our LC-Polscope measurements (Fig. 3 *A* and *B*), which is a strong confirmation of the theory, as this prediction is not based on a fit and in fact involves no parameters at all. We reproduced the observed spatial variation of polarity (23) by imposing vanishing polarity at the center of the spindle and fitting a single parameter given by the ratio of

polarity-dependent active transport and the preferred value of polarity due to motor activity (Fig. 3*C*; see *SI Text*). Finally, we calculated the aspect ratio of the spindle by balancing the active stress from motor activity with surface tension, which is a consequence of microtubules cross-linking each other. A surface tension of 143 ± 24 pN/μm reproduced an aspect ratio of 1.7 ± 0.5 and a shape that closely agrees with observation (see Fig. 3*D* and *SI Text*). This quantitative agreement between calculations and measurements demonstrate that local interactions between microtubules are sufficient to account for the morphology of the spindle.

The active liquid crystal theory of the spindle that our work has validated should be a powerful framework for understanding the spindle. The theory provides a basis for investigating the wide range of spindle phenomenology that has been observed, such as the fusion of two spindles (29) or the response of the spindle to physical perturbations (30). Molecular perturbations should act to change the parameters of the theory, such as K, the orientational elasticity, or W, the strength of the active stress, which could result in changes in spindle structure and dynamics. While additional work will be required to predict which parameters will be affected by specific molecular perturbations, this could be investigated empirically by using fluctuations to measure how molecular perturbations influence the theory's parameters. More broadly, the success of such a simple description demonstrates that, despite the extreme molecular complexity of spindles (31), their structure and dynamics at cellular scales are quantitatively accounted for using just a few effective parameters and argues that active liquid crystal theories are a promising route for developing predictive theories of cell biology (32).

Methods Summary

Spindle Assembly. We prepared CSF-arrested egg extracts from *Xenopus laevis* female oocytes as described previously (33). To measure microtubule density fluctuations, we added 0.5 μM Atto565-labeled tubulin to spindles and acquired 3D fluorescence movies. For two-point particle tracking, we added ∼100 pM Alexa647-labeled tubulin. We used a spinning disk confocal microscope (Nikon Ti2000), an EMCCD camera (Hamamatsu), and a 60× objective for acquisition of 3D fluorescence and two-point microrheology images. We used a LC-Polscope and a 100× objective for acquisition of orientation and retardance images.

Image Analysis. Before computing the spatiotemporal correlations, we registered spindles from a time lapse using a custom Matlab (The MathWorks) routine (34). For the two-point particle tracking measurements, we used custom-written Matlab code and routines from people.umass.edu/kilfoil/downloads.html (35).

Computation of Correlation Functions. We computed spatiotemporal correlations (3 space + 1 time for fluorescence and 2 space + 1 time for retardance movies) by first subtracting the temporal mean at each pixel of a time-lapse movie, and then using the periodogram formula $C(\vec{q},w) = F(\delta i(\vec{x},t))conj(F(\delta i(\vec{x},t))/V$, where δi is the fluctuation as a function of space and time, V is the product of time and space dimensions, and F is the discrete fast Fourier transform. We corrected for distortions in the empirically measured correlation functions due to the point spread function and finite exposure time by dividing the data by the Fourier transform and power spectrum of these response functions. When comparing theoretically predicted and measured correlation functions, we compensated for artifacts caused by calculating power spectra of finite data by analytically computing the expected periodogram of the theoretical prediction. Alternatively, applying different windowing functions to the data did not significantly change any of our results (36). We defined the cross-correlation of two pairs of tracer particles as $C_{\varepsilon\varepsilon}(R,t) = \frac{1}{2} < \varepsilon^{(1)}(t)\varepsilon^{(2)}(t) >$, where $\varepsilon^{(1)}$ and $\varepsilon^{(2)}$ are the displacements with respect to their initial position as a function of time of two tracer particles initially separated a distance R apart (see Fig. 1*E*). See *Stress Correlation Functions and Two-Point Microrheology*.

ACKNOWLEDGMENTS. We thank Andy Lau, Howard Stone, Frank Jülicher, Pierre Sens, Philippe Cluzel, and Reza Farhadifar for useful discussions, and Rudolf Oldenbourg and Grant Harris for assistance with the LC-Polscope. This work was supported by Nation Science Foundation Grants PHY-0847188 and DMR-0820484 and by the Human Frontiers Science Program.

1. Neumann B, et al. (2010) Phenotypic profiling of the human genome by time-lapse microscopy reveals cell division genes. *Nature* 464(7289):721–727.
2. Karsenti E, Vernos I (2001) The mitotic spindle: A self-made machine. *Science* 294(5542): 543–547.
3. Zheng Y (2010) A membranous spindle matrix orchestrates cell division. *Nat Rev Mol Cell Biol* 11(7):529–535.
4. Gadde S, Heald R (2004) Mechanisms and molecules of the mitotic spindle. *Curr Biol* 14(18):R797–R805.
5. Dumont S, Mitchison TJ (2009) Force and length in the mitotic spindle. *Curr Biol* 19(17):R749–R761.
6. Nédélec FJ, Surrey T, Maggs AC, Leibler S (1997) Self-organization of microtubules and motors. *Nature* 389(6648):305–308.
7. Sumino Y, et al. (2012) Large-scale vortex lattice emerging from collectively moving microtubules. *Nature* 483(7390):448–452.
8. Schaller V, Weber C, Semmrich C, Frey E, Bausch AR (2010) Polar patterns of driven filaments. *Nature* 467(7311):73–77.
9. Sanchez T, Chen DT, DeCamp SJ, Heymann M, Dogic Z (2012) Spontaneous motion in hierarchically assembled active matter. *Nature* 491(7424):431–434.
10. Sanchez T, Welch D, Nicastro D, Dogic Z (2011) Cilia-like beating of active microtubule bundles. *Science* 333(6041):456–459.
11. Kruse K, Joanny J-F, Jülicher F, Prost J, Sekimoto K (2004) Asters, vortices, and rotating spirals in active gels of polar filaments. *Phys Rev Lett* 92(7):078101.
12. Ramaswamy S (2010) The mechanics and statistics of active matter. *Annu Rev Condensed Matter Phys* 1:323–345.
13. Chaikin PM, Lubensky TC (2000) *Principles of Condensed Matter Physics* (Cambridge Univ Press, New York).
14. Oldenbourg R (1996) A new view on polarization microscopy. *Nature* 381(6585): 811–812.
15. Juelicher F, Kruse K, Prost J, Joanny J-F (2007) Active behavior of the cytoskeleton. *Phys Rep* 449(1-3):3–28.
16. Miyamoto DT, Perlman ZE, Burbank KS, Groen AC, Mitchison TJ (2004) The kinesin Eg5 drives poleward microtubule flux in *Xenopus laevis* egg extract spindles. *J Cell Biol* 167(5):813–818.
17. Aditi Simha R, Ramaswamy S (2002) Hydrodynamic fluctuations and instabilities in ordered suspensions of self-propelled particles. *Phys Rev Lett* 89(5):058101.
18. Crocker JC, et al. (2000) Two-point microrheology of inhomogeneous soft materials. *Phys Rev Lett* 85(4):888–891.
19. Lau AW, Hoffman BD, Davies A, Crocker JC, Lubensky TC (2003) Microrheology, stress fluctuations, and active behavior of living cells. *Phys Rev Lett* 91(19):198101.
20. Lau AWC, Lubensky TC (2009) Fluctuating hydrodynamics and microrheology of a dilute suspension of swimming bacteria. *Phys Rev E Stat Nonlin Soft Matter Phys* 80(1 Pt 1):011917.
21. Shimamoto Y, Maeda YT, Ishiwata S, Libchaber AJ, Kapoor TM (2011) Insights into the micromechanical properties of the metaphase spindle. *Cell* 145(7):1062–1074.
22. Heald R, Tournebize R, Habermann A, Karsenti E, Hyman A (1997) Spindle assembly in *Xenopus* egg extracts: Respective roles of centrosomes and microtubule self-organization. *J Cell Biol* 138(3):615–628.
23. Brugués J, Nuzzo V, Mazur E, Needleman DJ (2012) Nucleation and transport organize microtubules in metaphase spindles. *Cell* 149(3):554–564.
24. Needleman DJ, et al. (2010) Fast microtubule dynamics in meiotic spindles measured by single molecule imaging: Evidence that the spindle environment does not stabilize microtubules. *Mol Biol Cell* 21(2):323–333.
25. Mizuno D, Tardin C, Schmidt CF, Mackintosh FC (2007) Nonequilibrium mechanics of active cytoskeletal networks. *Science* 315(5810):370–373.
26. Mizuno D, Bacabac R, Tardin C, Head D, Schmidt CF (2009) High-resolution probing of cellular force transmission. *Phys Rev Lett* 102(16):168102.
27. Taylor G (1964) Disintegration of water drops in an electric field. *Proc R Soc London A* 280(1382):383–397.
28. Prinsen P, van der Schoot P (2003) Shape and director-field transformation of tactoids. *Phys Rev E Stat Nonlin Soft Matter Phys* 68(2 Pt 1):021701.
29. Gatlin JC, et al. (2009) Spindle fusion requires dynein-mediated sliding of oppositely oriented microtubules. *Curr Biol* 19(4):287–296.
30. Tirnauer JS, Salmon ED, Mitchison TJ (2004) Microtubule plus-end dynamics in *Xenopus* egg extract spindles. *Mol Biol Cell* 15(4):1776–1784.
31. Walczak CE, Heald R (2008) Mechanisms of mitotic spindle assembly and function. *Int Rev Cytol* 265:111–158.
32. Needleman D, Brugues J (2014) Determining physical principles of subcellular organization. *Dev Cell* 29(2):135–138.
33. Hannak E, Heald R (2006) Investigating mitotic spindle assembly and function in vitro using *Xenopus laevis* egg extracts. *Nat Protoc* 1(5):2305–2314.
34. Brugués J, Needleman D (2010) Nonequilibrium fluctuations in metaphase spindles: Polarized light microscopy, image registration, and correlation functions. *Proc SPIE* 7618:76180L.
35. Crocker J (1996) Methods of digital video microscopy for colloidal studies. *J Colloid Interface Sci* 179(1):298–310.
36. Austin RT, England AW, Wakefield GH (1994) Special problems in the estimation of power-law spectra as applied to topographical modeling. *IEEE Trans Geosci Remote Sens* 32(4):928–939.

Supporting Information

Brugués and Needleman 10.1073/pnas.1409404111

SI Text

Active Hydrodynamic Description of the Spindle

Hydrodynamic Equations. Spindles are primarily composed of microtubules and associated proteins that regulate the dynamics and interactions of microtubules. Our study focuses on spindles assembled in *Xenopus laevis* egg extracts, which recapitulate metaphase arrested meiosis II spindles. These spindles are on average ∼45 microns long and ∼30 microns wide. Microtubules in these spindles have an average length of ∼7 microns (1) and are at a density of ∼50–100 microtubules/μm^2 (2, 3), implying that there are ∼100,000 microtubules per spindle. Microtubules are polar polymers whose minus ends are relatively static and whose plus ends polymerize at a speed of ∼10–20 μm/min (4). There is no appreciable rate of rescues in these spindles (1), and the half-life of these microtubules is ∼16 s (5), much shorter than the typical lifetime of a spindle—which can exist for several hours. Microtubules in the spindle interact with each other via motors and cross-linkers, and continuously slide toward the poles at a rate of ∼2.5 μm/min (1, 6).

Microtubules in the spindle are deep within the nematic phase, as their volume fraction, ∼0.03, is well above the volume fraction at which the isotropic phase is expected to lose stability, ∼0.01 (7). While microtubules are uniformly highly aligned throughout the spindle (2), their net polarity varies spatially, ranging from antiparallel microtubules in the middle to most microtubules facing with their plus ends toward the center of the spindle near the poles (1). These observations suggest that it is necessary to use a polar field and a nematic field, both oriented along the same axis, to describe the ordering of microtubules in spindles. We choose a minimal model that is consistent with all of our data. In this model, the orientation of microtubules is determined by nematic interactions, and the polar field convects the microtubule concentration and polarity magnitude. The magnitude of the nematic field is taken to be constant throughout the spindle, while the magnitude of the polarity field depends on motor activity and self-advection (see below). This theory is consistent with a picture in which microtubules are oriented independent of the magnitude of their polarity, and microtubules are transported, polymerize, and depolymerize along the direction determined by their orientation. It is possible to construct more general theories involving both polar and nematic fields, but we consider the simplest theory that is consistent with all of our data. Our quantitative measurements are not compatible with pure nematic or pure polar theories (which, as discussed above, are also incompatible with the known symmetries of microtubules in the spindle).

We describe the hydrodynamic limit of the spindle with $\rho(\mathbf{x},t)$, the total density of microtubules (ρ_m) plus solvent (ρ_s), its total momentum $\mathbf{g}(\mathbf{x},t)$, nematic director orientation $\mathbf{n}(\mathbf{x},t)$, and polarity $\mathbf{p}(\mathbf{x},t)=p(\mathbf{x},t)\mathbf{n}(\mathbf{x},t)$. In what follows, we briefly describe the hydrodynamic equations for these variables.

We write the equation for the nematic and polar order parameter using the equations from liquid crystal physics with the appropriate symmetry, including terms not allowed in equilibrium, which arise from activity (8, 9),

$$\frac{\partial \mathbf{n}}{\partial t}=-\mathbf{v}\cdot\nabla\mathbf{n}+\Omega\mathbf{n}+\lambda\mathbf{A}\mathbf{n}+K\nabla^2\mathbf{n}, \qquad \text{[S1]}$$

$$\frac{\partial p}{\partial t}=-(\mathbf{v}+\lambda_1 p\mathbf{n})\cdot\nabla p+\left(\alpha-\beta p^2\right)p+\xi\mathbf{n}\cdot\nabla c+K_p\nabla^2 p, \qquad \text{[S2]}$$

where we have explicitly taken $\mathbf{p}=p\mathbf{n}$. The nematic equation includes advection by the hydrodynamic velocity $\mathbf{v}=\mathbf{g}/\rho$, with $\mathbf{g}$ the total momentum density, flow alignment of microtubules (8), $2\Omega\equiv\nabla\mathbf{v}-(\nabla\mathbf{v})^T$, and $2\mathbf{A}\equiv\nabla\mathbf{v}+(\nabla\mathbf{v})^T$, and liquid crystal elasticity in the one-Frank-constant approximation. The polar equation includes self-advection from polarity, two terms representing motor activity, which tend to fix a magnitude of polarity and modify polarity through gradients of concentration, and a diffusive term.

The equation for force balance reads

$$\partial_t g_j=\partial_j\left(\sigma^r_{ij}+\sigma^d_{ij}+\sigma^a_{ij}\right), \qquad \text{[S3]}$$

where the total stress is the sum of reactive, dissipative, and active stresses. Neglecting stress that explicitly depends on the magnitude of polarity,

$$\sigma^r=-\frac{\lambda}{2}\left(\mathbf{nh}+(\mathbf{hn})^T\right)+\frac{1}{2}\left(\mathbf{nh}-(\mathbf{hn})^T\right)-\Pi\mathbf{I}, \qquad \text{[S4]}$$

$$\sigma^d=\int_{-\infty}^{t}dt'\tilde{\mu}(t-t')\left(\nabla\mathbf{v}+(\nabla\mathbf{v})^T\right), \qquad \text{[S5]}$$

$$\sigma^a=Wc\left(\mathbf{nn}-\frac{\mathbf{I}}{d}\right). \qquad \text{[S6]}$$

The reactive term depends on an isotropic pressure and the molecular field $\mathbf{h}=K\nabla^2\mathbf{n}$ in the one-Frank-constant approximation and ignoring terms that depend on the magnitude of polarity; $\tilde{\mu}$ is the relaxation modulus, which we can estimate from ref. 10. For long time scales, the spindle is viscous, with a frequency-dependent viscosity (see *Stress Correlation Functions and Two-Point Microrheology*). The active stress is proportional to the nematic tensor and can be obtained by averaging the forces that the microtubules exert on the solvent (9, 11).

Microtubules polymerize by addition of tubulin dimers from the solvent. We assume that the interchange between solvent and microtubules does not involve volume changes and that the total density is conserved (more generally, these processes may involve changes in volume that in turn can create active stress, as in the case of cells growing in tissues) (12),

$$\frac{\partial\rho}{\partial t}+\nabla\cdot\mathbf{g}=0. \qquad \text{[S7]}$$

In terms of the microtubule concentration, $c\equiv\rho_m/\rho$,

$$\frac{\partial c}{\partial t}+\mathbf{v}\cdot\nabla c+\nabla\cdot\mathbf{j}=\Gamma(c,p), \qquad \text{[S8]}$$

where $\Gamma(c)$ is a source of microtubules, which includes microtubule nucleation and turnover, $\mathbf{v}=\mathbf{g}/\rho$, and the flux $\mathbf{j}=(\mathbf{v}_m-\mathbf{v}_s)\rho_s\rho_m/\rho^2$, where $\mathbf{v}_m$ and $\mathbf{v}_s$ are the microtubule and solvent velocities respectively; $\mathbf{j}$ can be obtained in the low-frequency limit from the difference between the microtubule and solvent current equations (11),

$$j_i=-\frac{\rho_m\rho_s}{2\rho^2\kappa}\partial_j\left(\sigma^m_{ij}-\sigma^s_{ij}\right)+\frac{\rho_m\rho_s}{\rho^2}v_p p_i-\frac{\rho_m\rho_s}{2\rho^2\kappa}W\partial_j c\left(n_i n_j-\delta_{ij}/d\right), \qquad \text{[S9]}$$

where $\mathbf{p}v_p$ is the average velocity of the microtubules arising from forces they exerted on the solvent. The first term is the passive

current that would exist in the absence of activity, and must be of the form $-D\nabla c$ (assuming that there are not forces acting selectively on solvent or particles). Substituting the current **j** into the equation for the microtubule concentration (Eq. **S8**) and keeping the lowest orders in microtubule orientation and concentration results in

$$\frac{\partial c}{\partial t}+\mathbf{v}\cdot\nabla c+\nabla\cdot[c\mathbf{p}v_0-D\nabla c]=\Gamma_0-\Theta c, \qquad \text{[S10]}$$

where v_0 is an effective velocity incorporating both movement from forces exerted on the solvent (v_p) and microtubule growth dynamics (possibly through microtubule-mediated microtubule nucleation, treadmilling, or plus-end dynamics). Θ is the effective turnover rate, and Γ_0 is a source term that generates microtubules.

Eqs. **S1**–**S3** and **S10** define the hydrodynamic limit of the spindle.

Spatiotemporal correlation functions. To test whether such a continuum description is appropriate for spindles, we obtain the equations for small fluctuations in the concentration, orientation, and stress, and derive the corresponding correlations to compare theoretical predictions with our measurements (see Fig. 2). To this end, we consider density fluctuations around a constant steady state (consistent with fluorescent images), $c=c_0+\delta c$. We consider a polar state for the spindle that changes very slowly along the spindle long axis (z), and therefore can be approximated by a constant for the region in which correlations are calculated. Polarity fluctuations are dominated by fluctuations in orientation, as fluctuations in magnitude relax much faster, so $\delta\mathbf{p}\sim p_0\delta\mathbf{n}_\perp$. Finally, we obtain the stress fluctuations as a function of fluctuations in density and orientation.

We derive the equation for orientation fluctuations $\delta\mathbf{n}_\perp$ from Eq. **S1**,

$$\frac{\partial\delta\mathbf{n}_\perp}{\partial t}-\hat{\mathbf{n}}_\perp(\delta\Omega+\lambda\delta\mathbf{A})\mathbf{n}_z-K\nabla^2\delta n_\perp=\hat{\mathbf{n}}_\perp\cdot\mathbf{S}, \qquad \text{[S11]}$$

where **S** is a random source of orientation with $\langle S(w,q)S(w',q')\rangle=S^2\delta(w+w')\delta(q+q')$. The term $\hat{\mathbf{n}}_\perp(\delta\Omega+\lambda\delta\mathbf{A})\mathbf{n}_z$ depends on hydrodynamic velocity fluctuations $\delta\mathbf{v}$, which we obtain from the force balance Eq. **S3**. Transforming in Fourier space, $\left(\int d\vec{x}\exp\left(i(\vec{q}\vec{x}-wt)\right)\right)$, and using the incompressibility condition, we find,

$$\delta\mathbf{v}=-i\frac{4}{3\eta q^2}W\left(\mathbf{q}_z\frac{q_\perp^2}{q^2}-\mathbf{q}_\perp\frac{q_z^2}{q^2}\right)\delta c \qquad \text{[S12]}$$

$$-i\frac{\beta}{q^2}\left[q_z\left(\mathbf{I}-2\frac{\mathbf{q}_\perp\mathbf{q}_\perp}{q^2}\right)\delta\mathbf{n}_\perp+\mathbf{q}_\perp\cdot\delta\mathbf{n}_\perp\left(\mathbf{I}-2\frac{\mathbf{q}_z\mathbf{q}_z}{q^2}\right)\mathbf{n}_z\right], \qquad \text{[S13]}$$

where $\eta=\mu^*/iw$ is a frequency-dependent viscosity (see *Stress Correlation Functions and Two-Point Microrheology*), and $\beta\equiv 1/\eta\,[Wc_0+q^2(\lambda K/2)]$. Since orientation measurements using the LC-Polscope are 2D (and integrated along the direction perpendicular to the plane, i.e., $q_x\approx 0$), we take $q_\perp=q_y$ parallel to $\delta n_\perp$, so that $\delta\mathbf{n}_\perp\cdot\mathbf{q}_\perp=\delta n_y q_y$. Experimentally, we measure the spatiotemporal correlation functions as a function of the wave number in the y direction (see Fig. 2) in the limit of $q_z\approx 0\ll q_y$. Within this limit, the term $\hat{\mathbf{n}}_\perp(\delta\Omega+\lambda\delta\mathbf{A})\mathbf{n}_z$ in the equation for the orientation fluctuations leads, after some algebra, to $(1+\lambda)\beta\delta n_y$ to leading order in q_z/q_y, and Eq. **S11** for the orientation fluctuations in Fourier space results in

$$\left(-iw+q_\perp^2K\right)\delta n_y-(1+\lambda)\beta\delta n_y=\hat{\mathbf{n}}_y\cdot\mathbf{S}. \qquad \text{[S14]}$$

We derive the equation for density fluctuations from Eq. **S10**. Taking the same limit as in the orientational fluctuations, $q_z\approx 0\approx q_x\ll q_\perp$ and $\delta\mathbf{n}_\perp\cdot\mathbf{q}_\perp=\delta n_y q_y$, the incompressibility condition $\mathbf{q}\delta\mathbf{v}\equiv 0$, neglecting gradients along the longitudinal direction in the magnitude of polarity ($v_0\delta c\partial_z p_0\ll c_0v_0p_0\partial_y\delta n_y$), and neglecting a potential noise source in the density fluctuations

$$\left(-iw+\Theta+Dq_y^2\right)\delta c+ic_0v_0'q_y\delta n_y=0, \qquad \text{[S15]}$$

where $v_0'=p_0v_0$. We assume $\Theta>0$ for stability. (Including a source of density fluctuations leads to an additive term in the correlation functions with a shape inconsistent with our measurements, which in turn can be explained only in terms of a source of orientational noise.) Combining Eqs. **S14** and **S15**, we find for the density fluctuations,

$$\left(-iw-\zeta+q_y^2K\right)\left(iw-\Theta-Dq_y^2\right)\delta c=ic_0v_0'q_yS_y, \qquad \text{[S16]}$$

where $\zeta\equiv(1+\lambda)\beta$. The dispersion relation reads $w=-iw_\pm(q)$, where $w_+(q)=\Theta+Dq_y^2$, and $w_-(q)=-\zeta+q_y^2K$. The stationary solution is stable only if $w_\pm$ is positive. The parameter ζ leads to instabilities (9) unless microtubule elasticity dominates at the larger length scales of the spindle, $|Wc_0/\eta|<Kq_{y0}^2$, with $q_{y0}\approx 0.39$ rad/μm. With the measured parameters, this condition is fulfilled provided the spindle width is smaller than ~ 150 μm (the typical width of a spindle is 20 μm). For the following analysis, we approximate $-\zeta+q_y^2K\approx q_y^2K$ (the estimated parameters obtained from what follows confirm that ζ is an order of magnitude smaller than Kq_y^2).

Orientation correlation functions. From Eq. **S14**, the spatiotemporal correlation function for the orientation fluctuations is

$$\langle\delta n_y(w,q)\delta n_y(-w,-q)\rangle=\frac{S_y^2}{w^2+K^2q_y^4}. \qquad \text{[S17]}$$

We compute the equal time orientation autocorrelation by integrating over frequencyx,

$$S_{nn}\equiv\frac{1}{2\pi}\int_{-\infty}^{\infty}dw\langle\delta n_y(w,q)\delta n_y(-w,-q)\rangle=\frac{S_y^2}{2Kq_y^2}. \qquad \text{[S18]}$$

Concentration correlation functions. The spatiotemporal correlation functions for the density fluctuations can be similarly obtained,

$$\langle\delta c(w,q)\delta c(-w,-q)\rangle=\frac{q_y^2v_0'^2c_0^2S_y^2}{\left(w^2+K^2q_y^4\right)\left(w^2+\left(\Theta+Dq_y^2\right)^2\right)}, \qquad \text{[S19]}$$

with corresponding static structure factor

$$S_{cc}=\frac{q_y^2v_0'^2c_0^2S_y^2}{2\left(K^2q_y^4+\left(\Theta+Dq_y^2\right)^2\right)}\left(\frac{1}{Kq_y^2}+\frac{1}{\Theta+Dq_y^2}\right). \qquad \text{[S20]}$$

There are three time scales involved in relaxation of concentration fluctuations: the characteristic turnover time $1/\Theta$, concentration diffusion $1/(Dq_y^2)$, and orientation diffusion $1/(Kq_y^2)$. For large wavelength fluctuations ($q_y\to 0$), relaxation by density and orientation diffusion becomes arbitrarily large, and any perturbation relaxes by microtubule turnover in the spindle, $\Theta\gg Kq_y^2, Dq_y^2$,

$$S_{cc}\sim\frac{c_0^2v_0'^2S_y^2}{2K\Theta^2}. \qquad \text{[S21]}$$

In the opposite limit, for small wavelengths, turnover is slower than relaxation by diffusion, $Kq_y^2, Dq_y^2\gg\Theta$, and

$$S_{cc} = \frac{c_0^2 v_0'^2 S_y^2}{2q_y^4} \frac{(D+K)}{KD(K^2+D^2)}. \quad \textbf{[S22]}$$

Finally, there is a possible intermediate regime in which turnover relaxes faster than concentration diffusion, but slower than orientation diffusion. In this regime, concentration fluctuations are driven by orientation fluctuations and the static structure factor decays as $1/q_y^2$, $Kq_y^2 \gg \Theta \gg Dq_y^2$,

$$S_{cc} = \frac{c_0^2 v_0'^2 S_y^2}{2K^2 \Theta q_y^2}. \quad \textbf{[S23]}$$

It is important to note that this last regime is possible only if $K \gg D$. Experimentally, we found that this regime is not present, indication that $D \approx K$.

Density–orientation correlation functions. The spatiotemporal cross-correlation between density and orientation fluctations is

$$\left\langle \delta c(w, q_y) \delta n_\perp(-w, -q_y) \right\rangle = \frac{-iv_0' c_0 q_y (-iw + \Theta + Dq_y) S_y^2}{\left(w^2 + K^2 q_y^4\right)\left(w^2 + \left(\Theta + Dq_y^2\right)^2\right)}, \quad \textbf{[S24]}$$

Leading to an equal time density–director cross-correlation function of

$$S_{cn} = \frac{-iv_0' c_0 S_y^2}{2Kq_y\left(\Theta + (K+D)q_y^2\right)}. \quad \textbf{[S25]}$$

When relaxation by turnover dominates, $\Theta \gg Dq_y^2, Kq_y^2$, and

$$S_{cn} \sim \frac{-iv_0' c_0 S_y^2}{2K\Theta q_y}. \quad \textbf{[S26]}$$

In the opposite limit, diffusion relaxation is faster than turnover, $(D+K)q_y^2 \gg \Theta$, and

$$S_{cn} \sim \frac{-iv_0' c_0 S_y^2}{2K(K+D)\Theta q_y^3}. \quad \textbf{[S27]}$$

Stress correlation functions and two-point microrheology. Two-point microrheology of active systems is related to the fluctuations of stress and the shear modulus of the continuum material, in this case the spindle, by (11)

$$C_{\varepsilon\varepsilon}(R, w) = \frac{\Delta(w)}{6\pi R \left|\mu(w)\right|^2}, \quad \textbf{[S28]}$$

where $C_{\varepsilon\varepsilon}(R, w)$ is the cross-correlation of pairs of tracer particles a distance R apart, $\Delta(w)$ is the active stress fluctuation spectrum in the long-wavelength limit, and $\mu(w)$ is the shear modulus. Despite the similarity in appearance, this relation is not based on the equilibrium fluctuation dissipation theorem, which is not applicable for active systems such as the spindle. Rather, Eq. **S28** results from linear response more generally and is valid for incompressible, viscoelastic continuous media in the presence of both active and thermal stress fluctuations (13, 11). The measured R^{-1} decay of $C_{\varepsilon\varepsilon}$ (Fig. 1*G*) shows consistency with Eq. **S28** and further argues that the spindle can be well described as a viscoelastic continuous media. Experimentally, we determined the cross-correlation of pairs of fluorescent molecules in the spindle by computing the correlation of each tracer displacement separated a distance R with respect to the initial position, $C_{\varepsilon\varepsilon}(R, t) = 1/2\left\langle \varepsilon^{(1)}(t)\varepsilon^{(2)}(t) \right\rangle$ along the perpendicular direction as a function of time; see Fig. 1*E*. This correlation in combination with measurements of the shear modulus performed by Shimamoto et al. (10) provides a measurement of the spectrum of active stress fluctuations $\Delta(w)$. Since the correlations are measured on the perpendicular direction, we need to calculate all of the contributions to stress correlations with components on the perpendicular direction. The full expression for these stress fluctuations is complex and has contributions from all terms in the total stress (Eqs. **S4**–**S6**), and we do not present its complete form here. However, for the interpretation of microrheology data, the relevant quantity is the stress fluctuations in the long-wavelength limit ($q = 0$). In this limit, the only nonvanishing contribution to the stress correlation comes from the active stress (Eq. **S6**) and is

$$\begin{aligned} \left\langle \delta\sigma_{yz}(0, w) \delta\sigma_{yz}(0, -w) \right\rangle &= 4W^2 c_0^2 \left\langle \delta n_y(0, w) \delta n_y(0, -w) \right\rangle \\ &= 4W^2 c_0^2 S_y^2 w^{-2} \equiv \Delta(w). \end{aligned} \quad \textbf{[S29]}$$

From Shimamoto et al. measurements, the stiffness $K(w) = K_0 w^{\beta_0}$, with $K_0 = 1.07 \pm 0.07$ nN/μm, and $\beta_0 = 0.39 \pm 0.04$. Taking into account the geometry of the glass needle used in their measurements, the stiffness is related to the shear modulus by $|K| = 8\pi a\mu/[\log(2a/b) + 1/2]$, where we considered the needle as an ellipsoid (14) of length a, the penetration length in the spindle ~30 μm, and width b ~2 μm, resulting in a shear modulus $\mu(w) = \mu_0 w^{\beta_0}$, with $\mu_0 = 5.5 \pm 0.4$ pN/μm^2. Since we measured the correlations of the tracers in real time, we express Eq. **S28** as a function of time,

$$\left|C_{\varepsilon\varepsilon}(R, t)\right| = \frac{4W^2 c_0^2 S_y^2}{6\pi^2 R \mu_0^2} \left|\sin\left[(-2 - 2\beta_0)\pi\right] t^{1+2\beta_0} \Gamma\left[-1 - 2\beta_0\right]\right|. \quad \textbf{[S30]}$$

We obtain the stress fluctuations using $\Delta(t) = 2W^2 c_0^2 S_y^2 t$,

$$\Delta(t) = \frac{C_{\varepsilon\varepsilon}(R, t) R \mu_0^2 3\pi^2}{\sin\left[(-2 - 2\beta_0)\pi\right] t^{2\beta_0} \Gamma\left[-1 - 2\beta_0\right]}. \quad \textbf{[S31]}$$

Spindle shape. We approximate the shape of the spindle as an ellipse with constant density and fixed volume. We search for a solution lacking hydrodynamic flow, v = 0, because: (*i*) the speed of movement of tubulin molecules in the spindle is independent of their distance from the spindle axis (1), suggesting that internal variations in v must be negligible; (*ii*) on occasion, a global flow of extract is present in samples (measured by flow of vesicles and other inhomogeneities in the cytoplasm), but, while the flow is retarded by the spindle and does not penetrate the spindle, the flow does not cause any deformation of spindle; thus, spindle morphology is insensitive to the presence of external flows; and (*iii*) the curl of the director field in the spindle is observed to be negligible (see below), arguing that internal circulating flows are not possible.

In the absence of hydrodynamic flows, the orientation Eq. **S1** is simply

$$\nabla^2 \theta(\mathbf{x}) = 0, \quad \textbf{[S32]}$$

which is coupled to force balance through the boundary conditions, taken to be given by tangential anchoring (see Fig. S1). Therefore, the orientation of microtubules in the spindle does not depend on any parameters in the theory and is determined solely be geometry. The solution of this equation for an ellipse with the same aspect ratio as the spindle quantitatively agrees with the orientation profile in the spindle measured using the LC-Polscope

(see Fig. 3 *A* and *B*), further validating the assumption of vanishing hydrodynamic velocity.

For the magnitude of polarity, we take the lowest order in gradients from Eq. **S2** in absence of hydrodynamic flows or density gradients,

$$-\lambda_1 p(z)\partial_z p(z) + \left(\alpha - \beta p(z)^2\right)p(z) = 0, \qquad \textbf{[S33]}$$

with solution $p(z) = \sqrt{\alpha/\beta}\tanh[(\sqrt{\alpha\beta}/\lambda_1)(z - L/2)]$, where L is the spindle length, and we have imposed $p(L/2) = 0$. We fit the profile of the magnitude of polarity fixing a maximum value for polarity of 1 ($\sqrt{\alpha/\beta} = 1$), which depends on the slope α/λ_1, (see Fig. 3*C*).

Following Taylor (15), we can obtain an equation for the aspect ratio of the spindle by considering the force balance at the central region and at the poles (see Fig. S1),

$$H\gamma = \sigma_{a\perp} - \Pi, \qquad \textbf{[S34]}$$

where γ is the surface tension of the spindle, $\sigma_{a\perp}$ is the normal active stress, and we have ignored nematic elasticity. H is the mean curvature, with values $2a/b^2$ and $ba^{-2} + b^{-1}$ at the pole and hemisphere, respectively. Solving for the pressure at these two points,

$$\gamma\left(2ab^{-2} - ba^{-2} - b^{-1}\right) = [\sigma_{a\perp}]_{z=a} - [\sigma_{a\perp}]_{z=0}. \qquad \textbf{[S35]}$$

The left-hand side can be rewritten as $\gamma(2\alpha^{-2/3} - \alpha^{5/6} - \alpha^{-1/6})/R_0$, where $\alpha = 1 - e^2 = a^2/b^2$, $e^2 = 1 - a^2/b^2$, and R_0 is the radius of a sphere with equal volume to the spheroid. At the hemisphere $(z = 0)$, the director is oriented in the z direction and $[\sigma_{a\perp}]_{z=a} = \sigma_{yy} + \sigma_{xy} + \sigma_{zy} = -(1/3)c_0 W$. $[\sigma_{a\perp}]_{z=0} = \sigma_{zz} + \sigma_{yz} + \sigma_{xz} = -(1/12)c_0 W$. In the last equality, we have calculated the average of this stress in a defect at the pole using $\langle n_z n_z\rangle = \frac{1}{\pi^2}\int_{-\pi/2}^{\pi/2}\int_{-\pi/2}^{\pi/2} d\phi d\theta \cos^2\theta \cos^2\phi = 1/4$, and $\langle n_x n_z\rangle = \langle n_y n_z\rangle = 0$.

The final equation for the aspect ratio of the spindle reads

$$\frac{R_0 c_0 W}{4\gamma} = -2\alpha^{-2/3} + \alpha^{5/6} + \alpha^{-1/6}. \qquad \textbf{[S36]}$$

From the shapes of both retardant and fluorescence spindles, we obtain α = 3.0 ± 0.5 (SE, n = 16), which is consistent with a surface tension $\gamma = 143 \pm 24$ pN/μm (SE from error propagation of error in α and $c_0 W$).

1. Brugués J, Nuzzo V, Mazur E, Needleman DJ (2012) Nucleation and transport organize microtubules in metaphase spindles. *Cell* 149(3):554–564.
2. Sato H, Ellis GW, Inoué S (1975) Microtubular origin of mitotic spindle form birefringence. Demonstration of the applicability of Wiener's equation. *J Cell Biol* 67(3):501–517.
3. Heald R, Tournebize R, Habermann A, Karsenti E, Hyman A (1997) Spindle assembly in *Xenopus* egg extracts: Respective roles of centrosomes and microtubule self-organization. *J Cell Biol* 138(3):615–628.
4. Tirnauer JS, Salmon ED, Mitchison TJ (2004) Microtubule plus-end dynamics in *Xenopus* egg extract spindles. *Mol Biol Cell* 15(4):1776–1784.
5. Needleman DJ, et al. (2010) Fast microtubule dynamics in meiotic spindles measured by single molecule imaging: Evidence that the spindle environment does not stabilize microtubules. *Mol Biol Cell* 21(2):323–333.
6. Miyamoto DT, Perlman ZE, Burbank KS, Groen AC, Mitchison TJ (2004) The kinesin Eg5 drives poleward microtubule flux in *Xenopus laevis* egg extract spindles. *J Cell Biol* 167(5):813–818.
7. Doi M, Edwards SF (1988) *The Theory of Polymer Dynamics* (Oxford Univ Press, New York).
8. de Gennes PG, Prost J (1993) *The Physics of Liquid Crystals* (Oxford Univ Press, New York).
9. Aditi Simha R, Ramaswamy S (2002) Hydrodynamic fluctuations and instabilities in ordered suspensions of self-propelled particles. *Phys Rev Lett* 89(5):058101.
10. Shimamoto Y, Maeda YT, Ishiwata S, Libchaber AJ, Kapoor TM (2011) Insights into the micromechanical properties of the metaphase spindle. *Cell* 145(7):1062–1074.
11. Lau AW, Lubensky TC (2009) Fluctuating hydrodynamics and microrheology of a dilute suspension of swimming bacteria. *Phys Rev E Stat Nonlin Soft Matter Phys* 80(1 Pt 1): 011917.
12. Ranft J, et al. (2010) Fluidization of tissues by cell division and apoptosis. *Proc Natl Acad Sci USA* 107(49):20863–20868.
13. Lau AW, Hoffman BD, Davies A, Crocker JC, Lubensky TC (2003) Microrheology, stress fluctuations, and active behavior of living cells. *Phys Rev Lett* 91(19):198101.
14. Berg HC (1993) *Random Walks in Biology* (Princeton Univ Press, Princeton, NJ).
15. Taylor G (1964) Disintegration of water drops in an electric field. *Proc R Soc London A* 280(1382):383–397.

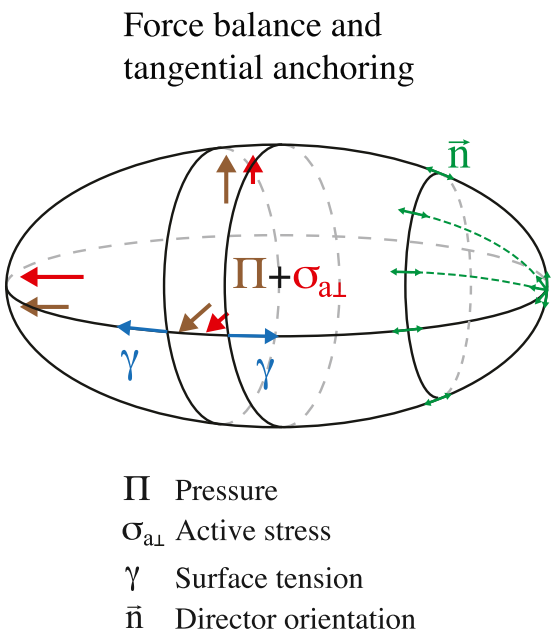

Fig. S1. Force balance and tangential anchoring, related to Fig. 3. Schematics of a spheroid representing the spindle. Forces due to normal components of active stress and pressure balance surface tension (brown, red, and blue arrows, respectively). Active stress is anisotropic, with a larger component along the longitudinal direction of the spindle. Microtubules are tangent to the boundary (green arrows) and form half defects at the poles.

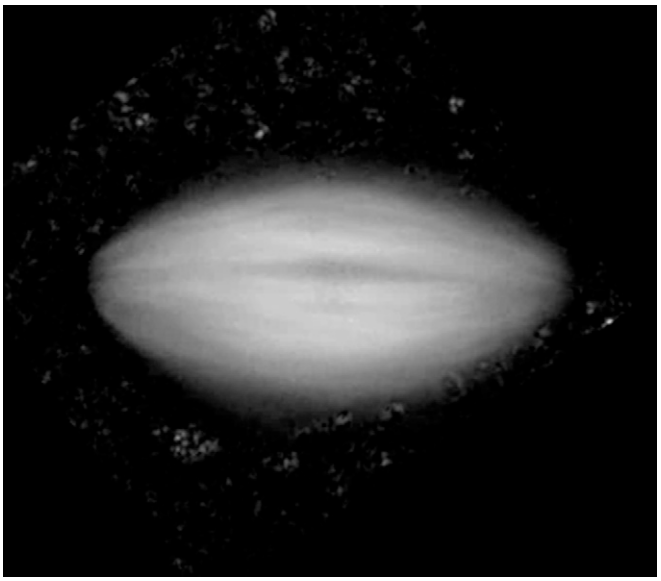

Movie S1. Retardance movie, related to Fig. 1. Time-lapse movie of the retardance from the LC-Polscope. Frame rate 1/4s; 50× speed.

Movie S1

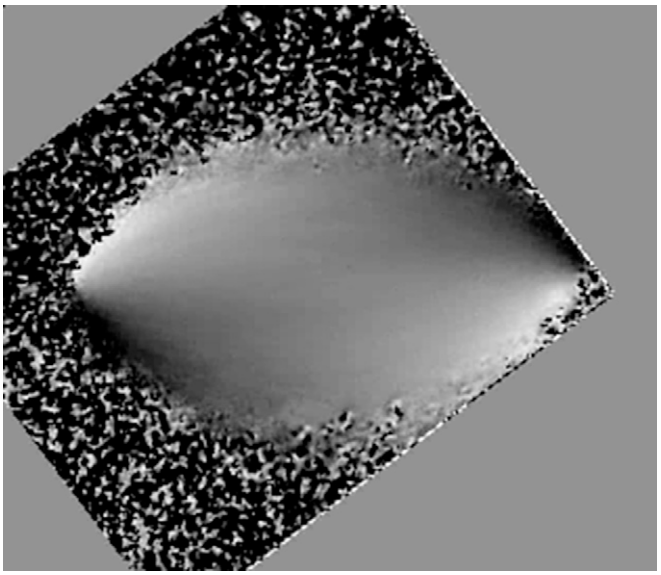

Movie S2. Slow axis movie, related to Fig. 1. Time-lapse movie of the slow axis from the LC-Polscope. Frame rate 1/4s; 50× speed.

Movie S2

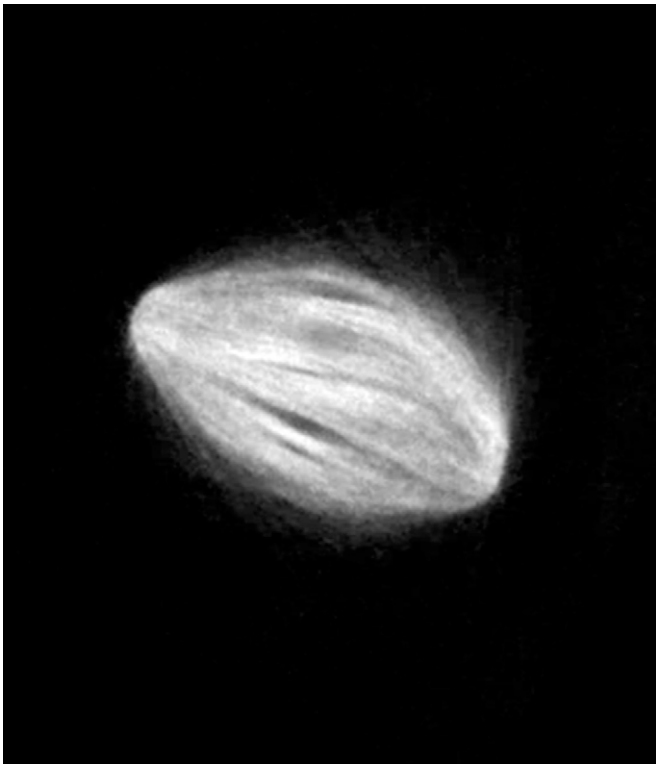

Movie S3. Fluorescence movie, related to Fig. 1. Slice of a 3D time-lapse movie of a spindle labeled with fluorescent tubulin. Frame rate 1/4s; 50× speed.

Movie S3

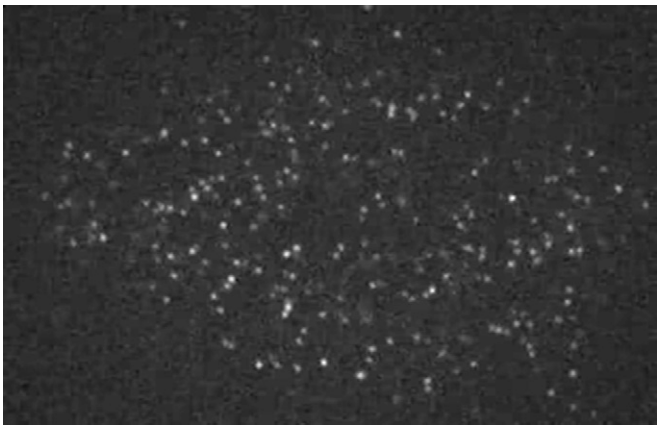

Movie S4. Single molecule movie, related to Fig. 1. Time-lapse movie of a spindle labeled with low density of fluorescent tubulin. Frame rate 1/2.1s; 50× speed.

Movie S4